INTERNATIONAL JOURNAL OF CIRCUIT THEORY AND APPLICATIONS
Int. J. Circ. Theor. Appl. 2009; **37**:505–528
Published online 18 November 2008 in Wiley InterScience (www.interscience.wiley.com). DOI: 10.1002/cta.567

The winnerless competition paradigm in cellular nonlinear networks: Models and applications

Paolo Arena[1], Luigi Fortuna[1], Davide Lombardo[1], Luca Patanè[1,*,†] and Manuel G. Velarde[2]

[1]*Dipartimento di Ingegneria Elettrica Elettronica e dei Sistemi, Università degli Studi di Catania, viale A. Doria 6, I-95125 Catania, Italy*
[2]*Instituto Pluridisciplinar, Universidad Complutense de Madrid, Paseo Juan XXIII 1, E-28040, Spain*

SUMMARY

Starting from the biological background on the olfactory architecture of both insects and mammalians, different nonlinear systems able to respond to spatial-distributed external stimuli with spatial–temporal dynamics have been investigated in the last decade. Among these, there is a class of neural networks that produces quasi-periodic trajectories that pass near heteroclinic contours and prove to be global attractors for the system. For this reason, these networks are called *winnerless competition* (WLC) networks. The sequence of saddle points crossed by each trajectory depends on the spatial input presented to the network and can be used as a 'code' representing a specific class of stimuli. Thanks to the intrinsic discrimination, WLC networks are often used for classification. In this paper, this capability is exploited within a framework for action-oriented perception. WLC networks are here used as bio-inspired architectures for the association between stimuli and 'percepts'. After presenting the theoretical basis of the WLC network in the classic Lotka–Volterra system, we investigate how WLC networks can be formalized in terms of cellular nonlinear networks (CNNs) hosting different kinds of cells: the FitzHugh–Nagumo neuron, the Izhikevich neuron and the single layer CNN standard cell. In order to find efficient ways to code environmental stimuli for action generation, we analyze and compare these WLC-based CNNs in terms of number of generated classes and robustness against the initial conditions. Based on the simulation results, we apply the best-performing system to solve a perceptual task involving navigation and obstacle avoidance. We demonstrate how the large memory capacity shown by the WLC–CNN is able to contribute to the new perceptual framework for autonomous artificial agents, where the association between stimuli and sequences is learned through the experience. Copyright © 2008 John Wiley & Sons, Ltd.

Received 18 September 2008; Accepted 2 October 2008

KEY WORDS: winnerless competition; perception; classification; dynamical neural networks

*Correspondence to: Luca Patané, Dipartimento di Ingegneria Elettrica Elettronica e dei Sistemi, Università degli Studi di Catania, viale A. Doria 6, I-95125 Catania, Italy.
†E-mail: lpatane@diees.unict.it

Contract/grant sponsor: European Commission
Contract/grant sponsor: MIUR-PRIN

1. INTRODUCTION

Recent neurophysiological studies have demonstrated the ability of animals to discriminate between similar but slightly different odors, which is crucial for the survival in a hostile environment. In particular, experiments on the mitral cells of the mammalian olfactory bulb [1] and on the projection neurons located within the insect antennal lobes [2] have shown that these neurons, involved in the second layer of sensation processing, are able to respond to different odors (or mixtures of odors) with repetitive and reproducible sequences of firing activity and quiescence [3]. Further, a deep analysis performed on the recorded activity of the 99 projection neurons of a locust antennal lobe [4] has shown how the transient dynamics of the neural activity are more effective in discriminate among different odors than the steady-state condition which, nevertheless, is reached after a certain amount of time. These resulting spatial–temporal patterns of activity are then projected toward the higher level processing centers like the mushroom bodies and the central complex, in the insect brain [5].

To model the behavior shown in the olfactory system, a class of dynamical systems was proposed in [6]: the winnerless competition (WLC) networks. These networks are able to transform a spatial-distributed input into a spatial–temporal pattern realized by a quasi-periodic trajectory that pass near a heteroclinic contour connecting saddle fixed points or saddle limit cycles, which corresponds to the firing state of a neuron (or a subgroup of neurons). Such a closed orbit represents a global attractor for the system [7] and, independently from the initial conditions, the trajectories tend asymptotically to it. It is to be emphasized that the results above mentioned, as also summarized in the following, were analytically formalized referring to three-species Lotka–Volterra systems (i.e. third-order dynamics). The same results were generalized referring only to autonomous n-species Lotka–Volterra systems, but, to the best of the author's knowledge, no analytical results were reported in the literature for general nth-order dynamics different from the Lotka–Volterra system. Therefore, no rigorous formalization has been derived for the WLC behavior in cellular nonlinear networks (CNNs) of nth dimension.

Based on these considerations, given that we need such a non-autonomous high-order dynamics to show the emergence of perceptual states, we'll refer to relevant neural models and for those ones we'll build CNN networks, deriving relevant conditions on the network parameters in order to show the emergence of WLC relevant behavioral characteristics, useful to fulfill our classification task. Referring to the classical WLC paradigm, the sequence of equilibria crossed by the trajectory depends on the stimulus and encodes the essential information relying on it. In this way, these main characteristics of WLC systems used for classification are:

- robustness to noise in the initial conditions,
- sensitivity to external stimuli,
- great number of possible classes.

Referring to the last feature, the advantage of this kind of approach with respect to coding with attractors in terms of capacity of the network is evident considering that in a multistable system, each class corresponds to a basin of attraction of one of the fixed points. Thus, for a system of N neurons with N stable fixed points (or limit cycle), the maximum number of possible classes is N. In a WLC network, the use of a transient dynamics in place of the steady-state equilibria greatly improves the number of possible classes; the number of sequences is potentially $e(N-1)!$ [6].

Starting from an analysis of the conditions for a Lotka–Volterra system to behave as a WLC network, in this work, given the lack of analytical WLC conditions, we investigate the conditions

DOI: 10.1002/cta

for qualitatively reproducing the behavior of a WLC network by using locally connected CNNs in which the basic cells belong to three classes: the FitzHugh–Nagumo (FHN) neuron [8], the Izhikevich (IZH) neuron [9] and the single layer CNN standard cells [10]. The choice of these three models was made to exploit the advantage of the WLC for different computational perspectives. FHN neurons can be used as a plausible model to reproduce many behaviors shown by the biological neurons, but introduce a high computational effort and can be used for computer simulation of a bio-inspired sensory system. Although showing many relevant neural characteristics, IZH neurons are less biological plausible, but not much time consuming and can be implemented in dedicated digital hardware [11] with the advantage of behavior flexibility as a function of the parameters used. The single layer CNN standard cells have the advantage of a straightforward and already existing analog hardware implementation [12]: this guarantees high performance in terms of computation time. On the other hand, CNNs have widely been demonstrated to be a paradigm for the generation and also learning of complex spatial–temporal dynamics [13], some of them derived by biological signals [14], even in single layer cells [15]. Moreover, complex spatial–temporal dynamics were shown to take place also in digital hardware implementations [16]. For the proposed systems, we studied how the sequence of active states is sensitive to the incoming stimuli and independent from initial conditions, underlining the high capacity of the networks. We also present a compact code representing each different sequence in order to extract from the spatial–temporal pattern a compact information as a code for the class associated with the current stimulus.

Finally, we propose an application demonstrating the possibility to use a WLC network in an artificial cognitive architecture in the challenging task of autonomous robot navigation where the ability to correctly interpret the incoming stimuli is crucial in the presence of unpredictable and potentially hostile situations. In particular, the WLC network plays the role of perceptual core within an already developed control architecture [17], which models the sensing-perception-action loop, where, instead of using an RD-CNN, we use a WLC network to generate the perceptual states, and consider, in place of the emerging Turing patterns, the spatiotemporal patterns coded by the sequence of activated neurons.

The sequence constitutes a compact representation of the surrounding environment and is associated with an action by a selection network. To perform a given task, the robot is provided with no *a priori* knowledge about the action to be associated with each pattern and learns by trial and error. Learning is implemented by two mechanisms: an unsupervised learning acts at the sensing block allowing the system to modulate the 'basins of attraction' of the sequences, while a simple reward-based reinforcement learning builds associations between spatiotemporal sequences and actions.

In the next section we will describe the WLC theoretical background in the classic Lotka–Volterra system, in Section 3, the different CNNs showing the WLC-like behavior are shown and analyzed, while in Section 4 we will present the application of one WLC network in a perceptual architecture for the autonomous navigation. Finally, in Section 5, we draw the conclusions and present the possible developments which are currently under investigation.

2. WLC IN LOTKA–VOLTERRA SYSTEM

In this section, we briefly review the principle of *WLC* network, which has been theoretically introduced through the Lotka–Volterra system described by the following equation in the case of

DOI: 10.1002/cta

N units and with the presence of external forcing (S_k):

$$\dot{x}_k = x_k \cdot \left(1 - x_k - \sum_{h=1, h\neq k}^{N} \rho_{k,h} \cdot x_h\right) + S_k \tag{1}$$

with $k = 1, \ldots, N$, and where $g_{k,h}$ are the coupling coefficients between the cells of the network. In order to have at least two different sequences, $N \geqslant 3$. To obtain a theoretical formalization, let us consider the simplest case, i.e. $N = 3$ and $S_k = 0$ $(k = 1, 2, 3)$ [7, 18, 19]

$$\begin{aligned} \dot{x}_1 &= f_1(x_1, x_2, x_3) = x_1(1 - x_1 - \alpha_1 x_2 - \beta_1 x_3) \\ \dot{x}_2 &= f_2(x_1, x_2, x_3) = x_2(1 - \beta_2 x_1 - x_2 - \alpha_2 x_3) \\ \dot{x}_3 &= f_3(x_1, x_2, x_3) = x_3(1 - \alpha_3 x_1 - \beta_3 x_2 - x_3) \end{aligned} \tag{2}$$

where $\alpha_1 = \rho_{1,2}$, $\alpha_2 = \rho_{2,3}$, $\alpha_3 = \rho_{3,1}$, $\beta_1 = \rho_{1,3}$, $\beta_2 = \rho_{2,1}$ and $\beta_3 = \rho_{3,3}$. The system has four classes of solutions:

- the origin, i.e. $x_1 = x_2 = x_3 = 0$,
- the axial fixed points, i.e. $x_k = 1$, $x_h = 0$ $(h \neq k)$,
- the planar fixed points, i.e. $x_k = 0$, $x_h \neq 0$ $(h \neq k)$,
- interior fixed point, i.e. $x_k \neq 0$ $(k = 1, 2, 3)$.

Assuming that $x_k > 0$ $(k = 1, 2, 3)$, neither $(0, 0, 0)$ nor the two-component equilibrium points are stable. Hence, we focus attention to the one-component equilibrium point $e_1 = (1, 0, 0)$, $e_2 = (0, 1, 0)$, $e_3 = (0, 0, 1)$ and to the remaining fixed point $p = (p_1, p_2, p_3)$. The stability of these solutions depends on the coupling coefficient α_i and β_i as shown by the Jacobian matrix:

$$J = -\frac{\partial f_k}{\partial x_h} = \begin{pmatrix} (1 - 2x_1 - \alpha_1 x_2 - \beta_1 x_3) & \alpha_1 x_1 & -\beta_1 x_1 \\ -\beta_1 x_2 & (1 - \beta 2x_1 - 2x_2 - \alpha_2 x_3) & -\alpha_2 x_2 \\ -\alpha_3 x_3 & -\beta_3 x_3 & (1 - \alpha_3 x_1 - \beta_3 x_2 - 2x_3) \end{pmatrix} \tag{3}$$

In the following subsections, we consider the possible dynamics shown by the system depending on the connection parameters.

2.1. Symmetric connections

In the case of symmetric connections, the system cannot generate complex temporal patterns. Rather, energy must decrease monotonically along any trajectory in state space or remains constant: the system can only move to a local minimum and stay there.

Two cases are possible:

- $\alpha_i = \beta_i = \rho$ $(i = 1, 2, 3)$,
- otherwise.

In the first case (symmetric and identical connections), the interior fixed point is

$$x_k = \frac{1}{1 + 2\rho} \tag{4}$$

with $k = 1, 2, 3$.

Note that this consideration can be extended to the case of N neurons obtaining for $k = 1, \ldots, N$:

$$x_k = \frac{1}{1 + \rho(N - 1)} \tag{5}$$

DOI: 10.1002/cta

Linearizing around each equilibrium and studying the stability, we can derive that, if $\rho<1$, the three one-component equilibrium points ($x_k=1$, $x_h=0$ if $h\neq k$) are saddles and the interior point is stable, vice versa if $\rho>1$, hence:

- if $\rho<1$, the system has $1/(1+2\rho)$ as global attractor (Figure 1),
- if $\rho>1$, the system has N stable fixed points $x_k=1$, $x_h=0$ with $h\neq k$ (Figure 2).

The first case is called *weak competition*, whereas the second one is referred as *multistability* for obvious reasons.

If the connections are symmetric, but not identical, (i.e. $\alpha_1=\beta_2=\rho$, $\alpha_2=\beta_3=\gamma$ and $\alpha_3=\beta_1=\delta$), the stability of both the one-component equilibrium points and fixed interior point depends on the three parameters, but also in this case we have:

- if $\rho,\gamma,\delta<1$ (or only one of these is greater than 1), the system has a global attractor with simultaneous, but not identical activity of all the neurons,
- if two among ρ,γ,δ are greater than one, the system has a global attractor corresponding to an identical activity of two cells,
- if $\rho,\gamma,\delta>1$, the 3 fixed points $x_k=1$, $x_h=0$ with $h\neq k$ are stable (Figure 2).

2.2. Asymmetric connections

In the case of asymmetric connections, for $N=3$, two cases arise:

- the system has a partial symmetry (e.g. $\alpha_1\simeq\beta_2$; $\beta_1,\alpha_2>1$; $\alpha_3,\beta_3<1$),
- the system has a strong asymmetry ($\rho_{k,h}\neq\rho_{h,k}$).

In the first case, the two state variables with quasi-symmetric connections mutually inhibit each other and the third one becomes active stabilizing at the value of 1 (Figure 3): this condition represents the global attractor for the system (*winner take all* condition).

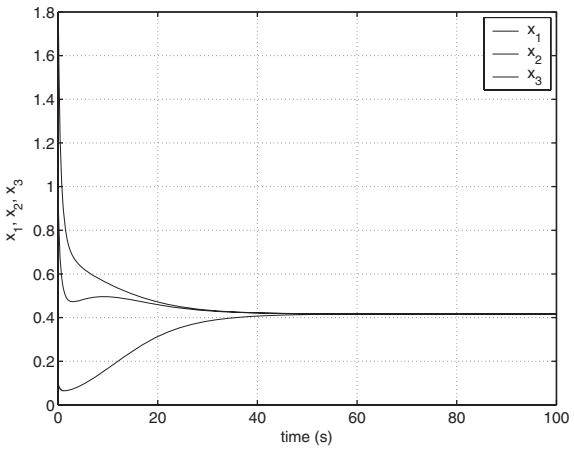

Figure 1. Behavior of the Lotka–Volterra system with $N=3$ and $\mathbf{S}=0$ when the coupling coefficients are symmetric, identical and *weak*: $\rho_{k,h}=\rho=0.7$, $k\neq h$.

DOI: 10.1002/cta

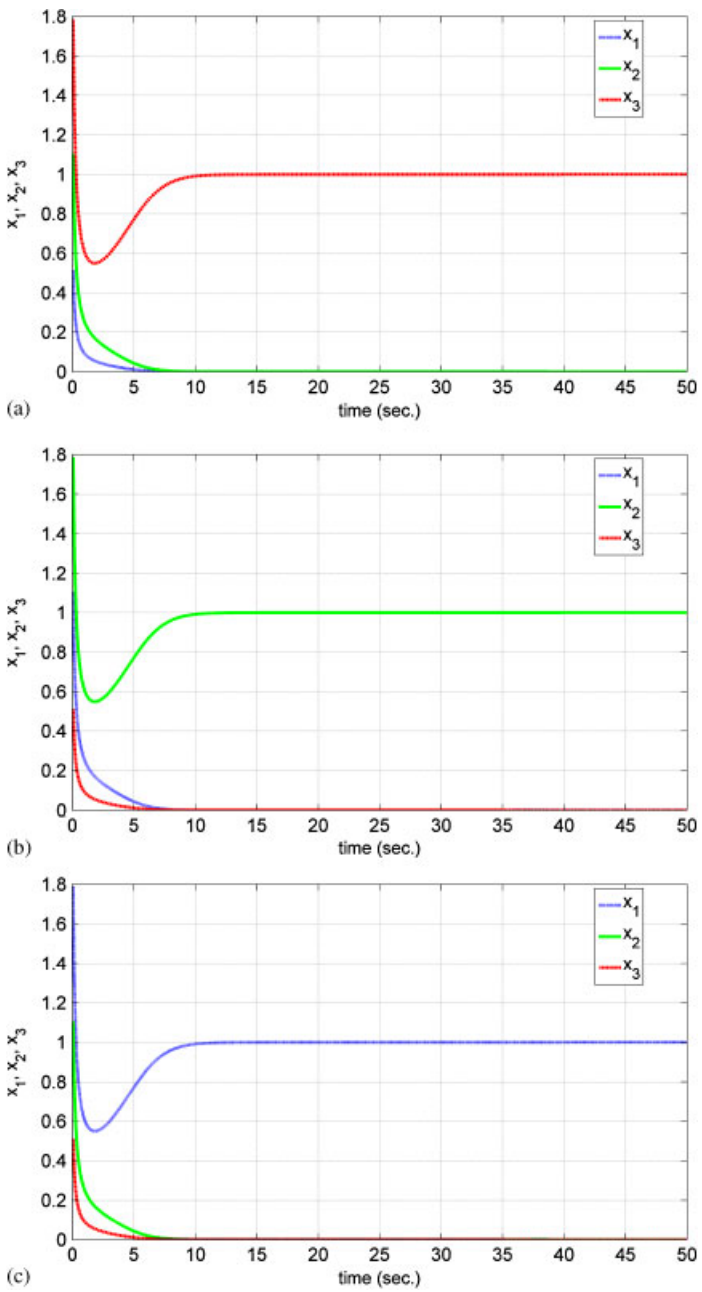

Figure 2. Behavior of the Lotka–Volterra system with $N=3$ and $\mathbf{S}=0$ when coupling coefficients are symmetric, identical and *strong*: $\rho_{k,h}=\rho=2$, $k\neq h$. The three pictures were obtained varying the initial conditions and demonstrate the multistability.

DOI: 10.1002/cta

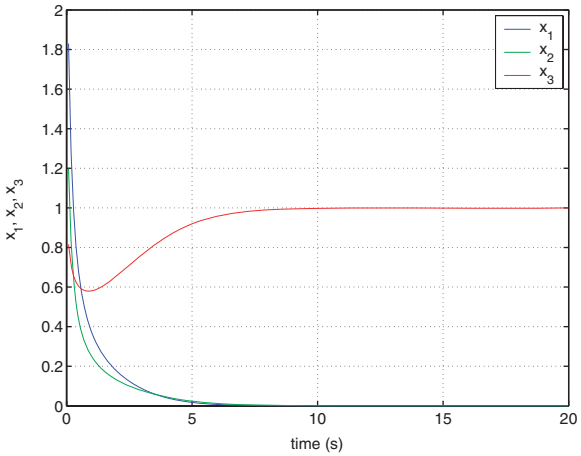

Figure 3. Behavior of the system with partially asymmetric connections (*winner take all*): $\rho_{1,2}=\rho_{2,1}=1.5$, $\rho_{1,3}=2$, $\rho_{3,1}=0.5$, $\rho_{2,3}=1.5$ and $\rho_{3,2}=0.5$.

In other terms, there are two unstable (saddle) points, corresponding to the activation of the two state variables with quasi-symmetric connections, and one stable fixed point, corresponding to the activation of the third state variable. The interior point is unstable.

In the second case, the three one-component equilibrium points are all saddle points of order 1 (two stable eigenvalues). Let us study the stability of the interior equilibrium point in simplified case of $\alpha_i=\alpha<1$ and $\beta_i=\beta>1$ $(i=1,2,3)$.

Case 1 $(1-\alpha)<(\beta-1)$: Hence the interior point is stable in the first direction, whereas in the other directions we have unstable orbits. The global behavior is a non-periodic albeit almost cyclic phenomena (Figure 4).

Case 2 $(\alpha+\beta=2)$: A Hopf bifurcation occurs and there is a family of neutrally stable periodic solutions and a limit cycle branches from the fixed point.

Case 3 $(\alpha+\beta<2)$ *with* $\alpha<1$ *and* $\beta>1$: Hence, the interior fixed point is stable and the system converges to it.

If we define the parameter $\kappa_i=(\beta_i-1)/(1-\alpha_i)$ $(i=1,2,3)$, we can classify the behavior into three cases: (1) $\kappa_1\kappa_2\kappa_3>1$, then a heteroclinic contour consists of saddle equilibrium points and separatrices connecting these equilibria. The contour can serve as an attracting set if every saddle point has only one unstable direction; (2) $\kappa_1\kappa_2\kappa_3>1$, if a small disturbance is able to destroy the heteroclinic orbit, then a stable limit cycle appears in its proximity where exists a family of neutrally stable periodic solutions; (3) $\kappa_1\kappa_2\kappa_3<1$: the interior point becomes a global attractor.

The case (1) is defined as *WLC* case, because from every initial condition, the trajectory is attracted by one of the one-dimensional fixed points, then escapes along the only unstable direction toward another saddle. Thus, the sequence of saddles crossed by the trajectory does not depend on the specific initial condition, but is 'written' in the connection parameters.

In the next section, we extend the case to more complex networks where the connection parameters are fixed, but the presence of an additive term, as external forcing, is able to determine the sequence that plays the role of global attractor for the system.

DOI: 10.1002/cta

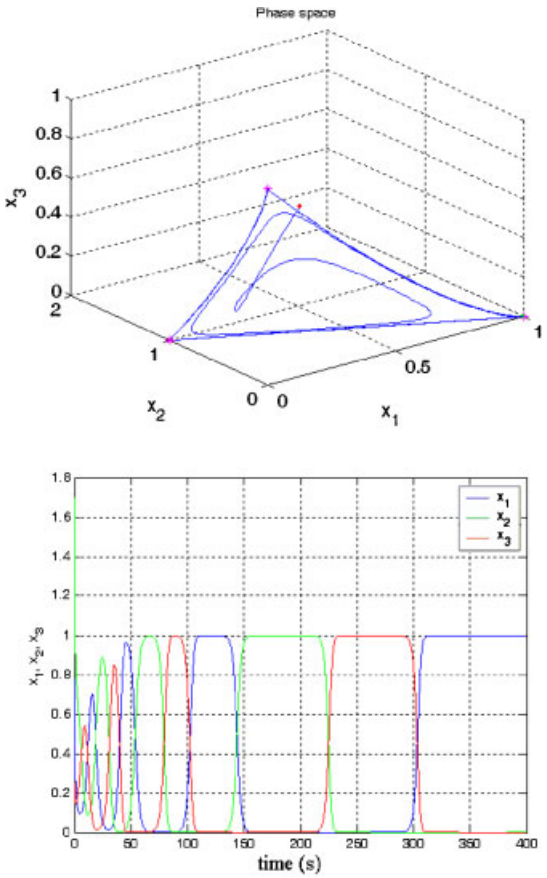

Figure 4. Behavior of the system with strongly asymmetric connections (*winnerless competition*): $\rho_{1,2}=1.5$, $\rho_{1,3}=\rho_{2,1}=\rho_{3,2}=0.5$, $\rho_{2,3}=\rho_{3,1}=2$.

3. WLC-LIKE BEHAVIOR IN CNNs

In this section, we show how the WLC principle can be extended to dynamical systems representing biologically plausible neural networks, which are activated by the presence of external stimuli and quiescent otherwise

$$\dot{\mathbf{x}}_k = f(\mathbf{x}) - \sum_{h=1,h\neq k}^{N} G_{k,h}(\mathbf{S})\cdot[x_k^1, x_h^1] + S_k \tag{6}$$

with $k=1,\ldots,N$ and where:

- N is the number of neurons in the network,
- $\mathbf{x}_k$ is the vector of the state variables of the neuron k,
- $f(\cdot)$ is a nonlinear function
- $G_{k,h}\cdot[\cdot,\cdot]$ describes the inhibitory effect of the neuron h onto neuron k,

DOI: 10.1002/cta

- x_k^1, x_k^1 are the state variables describing the membrane potential of the neuron k and h, respectively,
- $\mathbf{S}$ is the vector of the external forcing, and S_k is the kth component of $\mathbf{S}$.

In a system belonging to this class, the external stimuli $\mathbf{S}$ act onto the inhibitory connections between the neurons and/or as an additive forcing.

As already outlined, the theoretical formalizations of the WLC have been originally shown in the three-species Lotka–Volterra system. The extension to the case of a nonlinear system in the general form of 3 is at the basis of the exploitation of the WLC behavior in CNNs. This extension leads to the loss of a *general* rigorous demonstration of the WLC conditions, even if the main dynamics of such systems is captured by the Lotka–Volterra system [6]. In order to theoretically prove the WLC behavior for a *specific* nonlinear system, i.e. after setting the dynamics of the cells and the stimuli patterns, a possible way to follow is suggested in [7], where the authors demonstrated the existence and the stability of the heteroclinic contour in the case of nth-order Lotka–Volterra system, even if only in the case of autonomous equations. However, a rigorous demonstration of the WLC behavior for a specific system is outside the scope of this work, which aims at exploiting the potentialities of the CNN as a nonlinear dynamic classifier when showing a *WLC-like* behavior, i.e. a fixed sequence of cell activation dynamics, as a function of the external input.

Under these considerations, we propose a heuristic definition of a *WLC-like* behavior based on the main features derived in [3, 6]. Therefore, in terms of phase space behavior, a system can be defined as a WLC network when:

- the trajectories evolve near a heteroclinic orbit crossing unstable states,
- the sequence of the unstable equilibria crossed is sensitive to the stimuli,
- given the stimuli, the trajectory obtained is a global attractor for the system.

In this paper, we extend the WLC principle to the class of $2D$ 3×3 locally connected CNNs. To do this, we consider the case of $G_{k,h}(\mathbf{S})=g_{k,h}$, i.e. independent from the external stimuli $\mathbf{S}$. The choice for the strength of the inhibitory connections $g_{j,i}$ has to reflect the considerations for the asymmetry that triggers the WLC behavior in the Lotka–Volterra system. A possible configuration for the parameters is graphically represented by the topology of Figure 5. In fact the 9×9 inhibitory connection matrix, which corresponds to the topology, proves to be strongly asymmetric, as we reported below:

$$\mathbf{g}=\begin{pmatrix} 0 & g_2 & 0 & 0 & g_1 & 0 & 0 & 0 & 0 \\ g_1 & 0 & 0 & g_1 & g_2 & g_1 & 0 & 0 & 0 \\ 0 & 0 & 0 & 0 & g_2 & g_1 & 0 & 0 & 0 \\ 0 & g_2 & 0 & 0 & g_1 & 0 & g_2 & g_2 & 0 \\ b & g_1 & g_1 & g_2 & 0 & g_2 & g_1 & g_1 & g_2 \\ 0 & g_2 & g_2 & 0 & g_1 & 0 & 0 & g_2 & 0 \\ 0 & 0 & 0 & g_1 & g_2 & 0 & 0 & 0 & 0 \\ 0 & 0 & 0 & g_1 & g_2 & g_1 & 0 & 0 & g_1 \\ 0 & 0 & 0 & 0 & g_1 & 0 & 0 & g_2 & 0 \end{pmatrix} \tag{7}$$

Although many different choices are possible with $g_1>g_2$ or vice versa, we set $g_1=2$ and $g_2=0$ for all the simulations presented in the following.

DOI: 10.1002/cta

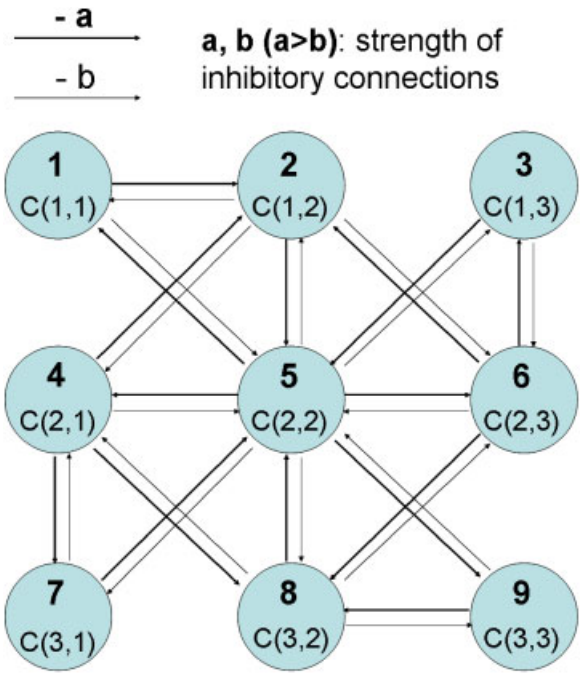

Figure 5. Topology of a $2D$ 3×3 cellular nonlinear network with asymmetric connection. The solid arrows represent inhibitory connections between the cells with a strength a, whereas the thin arrows refer to inhibitory connection with strength b.

As stated above, the specific dynamics of each cell can be chosen in different ways; hence, in the following subsection, we will implement the network with three kinds of neurons: the FHN neurons, the IZH neurons and the single layer CNN standard cells for the reasons discussed in the introduction.

3.1. FHN neurons

The first case is a network of 3×3 locally connected FHN neurons [8], where each cell (i, j) of the network is represented by a third-order nonlinear system

$$\begin{aligned}\tau_1\dot{x}_{i,j} &= f(x_{i,j})-y_{i,j}-z_{i,j}\cdot(x_{i,j}-v)+0.35+S_{i,j}\,\dot{y}_{i,j}=x_{i,j}-by_{i,j}+a\\ \tau_2\dot{z}_{i,j} &= \sum_{C(k,l)\in N_1(i,j)} g_{kl,ij}G(x_{k,l})-z_{i,j}\end{aligned} \tag{8}$$

with $i, j=1,2,3$, where $g_{kl,ij}$ is the strength of the inhibitory connection of the cell $C(i, j)$ on the cell $C(k, l)$ and where

$$N_1(i, j)=C(k, l)|\max(|k-i|; |l-j|)<1 \tag{9}$$

with $k, l=1,2,3$, where $C(k, l)$ is the cell of position (k, l) and N_1 is the *neighborhood of radius* 1.

DOI: 10.1002/cta

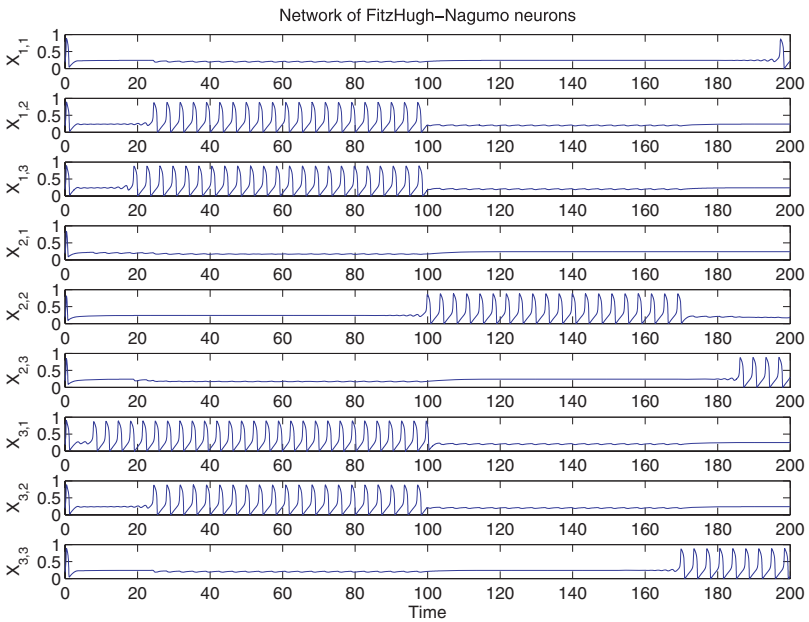

Figure 6. Dynamics of the first state variable of each FHN neuron used in the 3×3 network reported in Figure 5, in presence of the set of constant stimuli $S_1 = [0, 0, 0.01, 0, 0, 0.01, 0.05, 0, 0.01]$ for 200 s of simulation. The amplitude of the variables was scaled in the range $[0, 1]$.

For each cell $C(i, j)$:

- $x_{i,j}$ is the membrane potential,
- $y_{i,j}$ is the recovery variable,
- $z_{i,j}$ is the synaptic current modeled by a first-order dynamics,
- $f(x_{i,j}) = x_{i,j} - \frac{1}{3}x_{i,j}^3$ is the FHN neuron internal nonlinearity,
- $S_{i,j}$ is the external stimulus to neuron i, j,
- $G(x_{i,j})$ is the Heaviside function.

The parameters used in the simulations were $a = 0.7$, $b = 0.8$, $\tau_1 = 0.08$, $\tau_2 = 4.1$, $v = -1.5$.

The behavior of the network with the chosen parameters proves to be strongly influenced by the input and marginally by the initial conditions, demonstrating a WLC-like behavior. Figure 6 depicts the dynamics of the network: in general, each neuron shows resting phases alternating with the activation phases in which they fire (spiking or bursting). After a transient phase, the activation sequence among the neurons maintains constant; hence, it is possible to code the sequence of activation of the neurons following the temporal order, i.e. in the example 7-3-1-8-2-5-4-9. This sequence is made up by the activation of eight neurons, being neuron six always quiescent.

3.2. IZH neurons

Another possible neuron model that has been used was proposed by IZH [9], which is able to reproduce almost all the possible dynamics of the biological neurons with the computational

DOI: 10.1002/cta

effectiveness of the integrate-and-fire neuron. The cell of the network has, in this case, the form

$$\begin{aligned} \dot{x}_{i,j} &= 0.04x_{i,j}^2 + 5x_{i,j} + 140 - y_{i,j} + I_{i,j} \\ \dot{y}_{i,j} &= a(bx_{i,j} - y_{i,j}) \\ \dot{z}_{i,j} &= \sum_{C(k,l)\in N_1(i,j)} g_{kl,ij} G(x_{k,l}) - z_{i,j} \end{aligned} \tag{10}$$

with the spike-resetting:

$$\text{if } x_{i,j} \geqslant 30\,\text{mV} \quad \text{then} \begin{cases} x_{i,j} \leftarrow c \\ y_{i,j} \leftarrow u + d \end{cases} \tag{11}$$

$$N_1(i,j) = C(k,l) | \max(|k-i|; |l-j|) < 1 \tag{12}$$

with $k, l = 1, 2, 3$, where $C(k,l)$ is the cell of position (k,l) and N_1 is the *neighborhood of radius* 1.

Again, $x_{i,j}$, $y_{i,j}$ are dimensionless variables representing the neuron's membrane potential and the recovery variable, $I_{i,j}$ is the input current, whereas a, b, c and d are system parameters that determine the kind of dynamics showed by the neuron.

To obtain both dynamics similar to the one shown by the FHN network and a WLC-like behavior, the parameters have been chosen experimentally among the model for the phasic bursting behavior [9] and in particular they are: $a = 0.05$, $b = 0.28$, $c = -50$, $d = 0.05$. Figure 7 shows the dynamics of a 3×3 network with these parameters for a given choice of the external stimuli.

3.3. Single layer CNN standard cells

Alternatively, to implement a cell of the network, it is possible to use a less biologically realistic (but straightforward to be implemented) first-order system that corresponds to the traditional CNN standard cell [10]

$$\begin{aligned} \dot{x}_{i,j} &= -x_{i,j} + \sum_{C(k,l)\in N_1(i,j)} A^{i,j} y_{k,l} + B^{i,j} u_{i,j} \\ y_{i,j} &= 0.5(|x_{i,j} + 1| - |x_{i,j} - 1|) \end{aligned} \tag{13}$$

with $i, j = 1, 2, 3$ and where

$$N_1(i,j) = C(k,l) | \max(|k-i|; |l-j|) < 1 \tag{14}$$

with $k, l = 1, 2, 3$, where $C(k,l)$ is the cell of position (k,l) and N_1 is the *neighborhood of radius* 1. The additive stimuli are represented by the $u_{i,j}$ inputs to the CNN.

Using this network, we have the advantage of much reduced computational effort and possible hardware realization [12].

The WLC-like behavior of the first-order CNN standard cell for both a network of three cells and a 3×3 system was shown in [20] where the 9×9 connection matrix is reported in terms of space-varying templates A and space-invariant template B.

DOI: 10.1002/cta

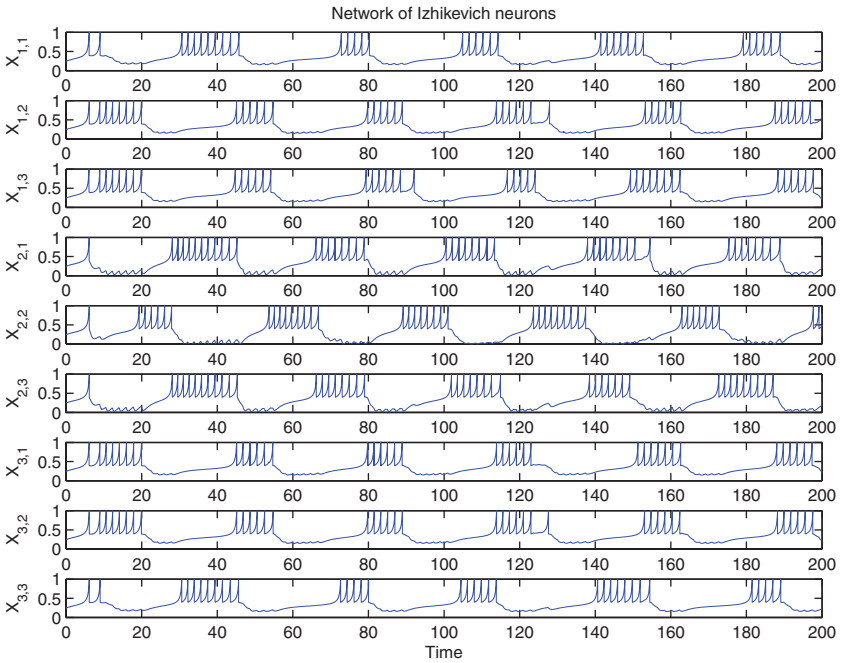

Figure 7. Dynamics of the first state variable of each Izhikevich neuron, used in the 3×3 network reported in Figure 5, in the presence of the set of constant stimuli $S_1 = [0, 0, 0.01, 0, 0, 0.01, 0.05, 0, 0.01]$ for 200 s of simulation. The amplitude of the variables was scaled in the range $[0, 1]$.

The dynamics of the cells of the 3×3 network are shown in Figure 8.

3.4. Coding the heteroclinic orbit

The heteroclinic orbit depends on the external forcing, thus any set of input stimuli can be classified by using the resulting orbit as a code representing a class.

A possible choice for the code to be associated with the trajectory shown by the WLC-like systems is obtained by looking at the activation timing of each cell. In this way, the sequence $m-n-p$ means that the cell m is the first to *fire*, the cell n is the second and cell p is the third one. Extending the code to the more complex and larger networks, if the number of cells in the network is less than 9 a simple integer code can be associated with each sequence simply by enumerating the cells. Hence, if, in the case of the three neurons network, cell m is represented by 1, cell n by 2 and cell p by 3 the sequence becomes 1-2-3. It should be noticed that 1-2-3, 2-3-1 and 3-1-2 constitute the same sequence. To have a unique representation for any sequence, we will code any sequence starting from the smallest number (e.g. for the previous case, we will choose 1-2-3 as the code). In case of the 3×3 system proposed in the previous subsections, it is necessary to handle the synchronization between two or more cells. To do this, if both the activation times of two cells of the network fall in a small pre-defined time window, we consider the two cells synchronized and we order them in the code starting from the smallest.

DOI: 10.1002/cta

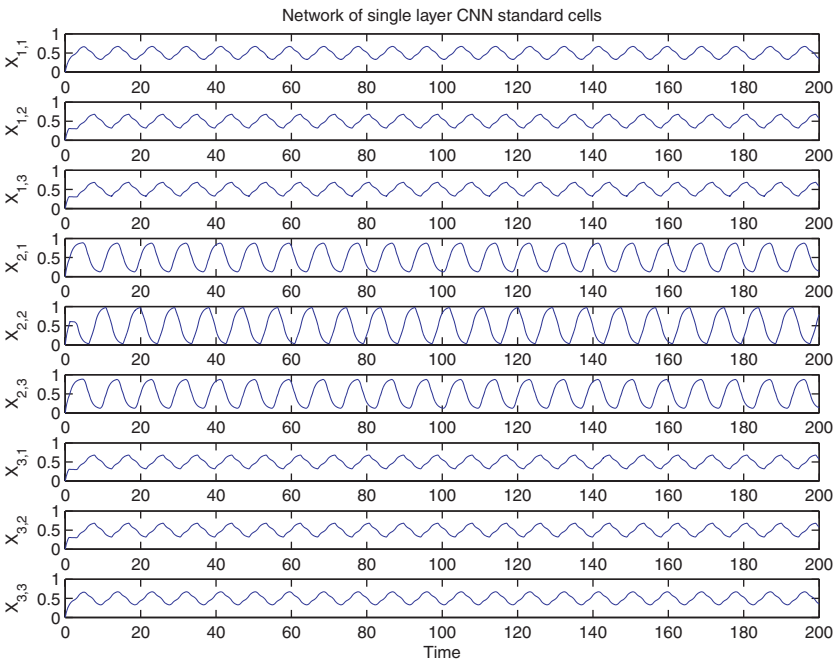

Figure 8. Dynamics of the first state variable of each single layer CNN standard cell, used in the 3×3 network reported in Figure 5, in the presence of the set of constant stimuli $S_1 = [0, 0, 0.01, 0, 0, 0.01, 0.05, 0, 0.01]$ for 200 s of simulation. The amplitude of the variables was scaled in the range $[0, 1]$.

This coding mechanism is a slight simplification of the one proposed in [20] and reduces the number of classes, which can be distinguished, but is less expensive in terms of computational effort and memory.

3.5. Classification performance of the systems

In this subsection, we explore the classification performance of the three proposed networks in terms of number of classes, computational effort and robustness (repeatability).

With this aim, we scaled the dynamics of the first state variables of all the systems in the range $[0, 1]$ and let the external stimuli vary in the nine-dimensional hypercube $[0, 0.2]^9$, where the first two systems have a busting behavior, while the cells of the single layer CNN show oscillations between a high and a low level, and we randomly choose 500 sets of stimuli belonging to this region. Then, for each system, we perform a simulation made of 500 trials varying the additive term according to the previous choice setting the initial conditions at a fixed value and then repeating the experiment varying the initial conditions at each trial. The results are summarized in Table I.

The misclassification rate, i.e. the percentage of codes resulting to be different in the trials with different initial conditions, could seem to be quite high (in Table I we refer to *robustness* to indicate the inverse of misclassification rate). Nevertheless, most of the misclassifications occur at the boundary between two classes and could be solved with a better choice of the code, which in

DOI: 10.1002/cta

Table I. Classification performance of the three proposed networks: the FitzHugh–Nagumo networks, the Izhikevich networks and the one layer CNN.

System	Classes	Robustness (%)	n. flops
FHN	402	81	$22+2*8$
IZH	27	40	$20+2*8$
CNN	3	91	$9+6*8$

The column *Classes* indicate the total number of different classes emerged in the 500 trials made varying the set of stimuli, whereas the column *Robustness* refers to percentage of the total trials where the sequence emerged using fixed initial conditions resulted to be equal to the one evaluated starting from initial conditions randomly chosen in the range $[0, 1]$. Finally, *n. flops* is the number of floating point operations needed for the integration step of one cell.

this case does not completely allow to guarantee the robustness of the classification. The results demonstrate how the FHN network presents the highest number of possible classes with a good robustness, a medium number of floating point operations for a digital implementation, while it is heavy to implement in hardware due to the cubic operator. The IZH network has much less classes and it is much less robust against variations in the initial conditions, even if it has the least number of floating points operations. The CNN is very poor in terms of number of classes, but very robust against variation in the initial conditions. The latter features and the existence of the hardware chip [12] make it the best solution for an analog hardware implementation for applications where a little number of classes is enough. It should be noticed that the number of sequences of both the CNN and the IZH network would double if the hypercube is enlarged to the negative values, while all the systems slightly increase the number of classes if the hypercube is enlarged to higher positive values.

In order to provide a graphical overview of the classification of the external stimuli performed by the three systems, we consider a bi-dimensional subsection of the space of the stimuli and show the different sequences emerged varying the stimuli within this region. In particular, we chose to vary the stimuli associated with *neuron 2* and *neuron 7* and keep fixed the value of the stimuli in the other seven neurons. For the two selected neurons, the stimuli, referred in the following as $S_{1,2}$ and $S_{3,1}$, were varied in different range for the three systems in order to exploit their features. In particular, it should be noticed that the system with single layer CNN standard cells maintains a WLC-like behavior in the largest range. In any case, we divide the range of variation of the stimuli in 21 steps, thus for each system, we performed $21 \times 21 = 441$ trials in our simulation, evaluating the code from the resulting sequence. Figures 9–11 show the results of the simulations for the three systems. It should be noticed how the geometry of the classes presents a high regularity in the case of FHN neurons and single layer CNN standard cells, while they are very 'disordered' in the case of IZH neurons.

4. APPLICATION TO PERCEPTUAL ARCHITECTURE

The results about the classification performance of the three systems lead us to choose the FHN system, even if the digital implementation prevents us from the misclassifications and the IZH system is the least time consuming in this domain. Indeed, the highest number of possible classes

DOI: 10.1002/cta

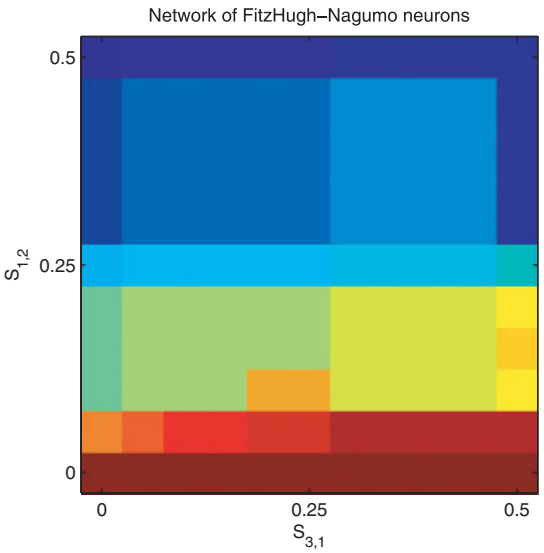

Figure 9. Network of FitzHugh–Nagumo neurons: results of the simulation obtained varying the stimuli for the neuron 2 and for the neuron 7 in the range $[0, 0.5]$ (step of 0.025) and keeping fixed to 0 the stimuli for the other cells. The number of classes emerged is 32 for the 441 trials.

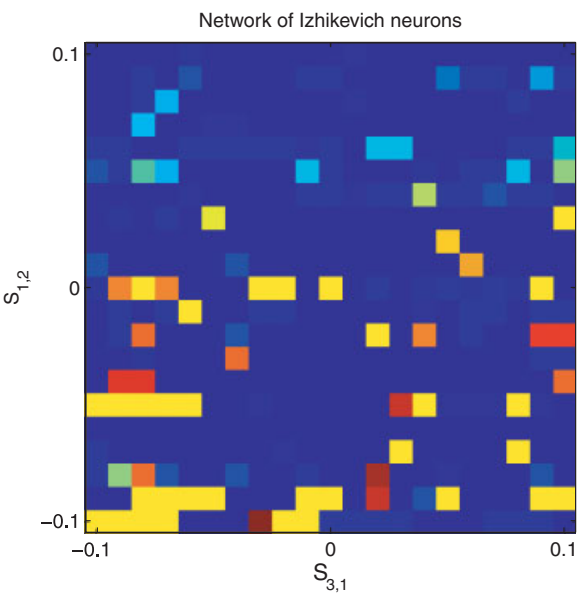

Figure 10. Network of Izhikevich neurons: results of the simulation obtained varying the stimuli for the neuron 2 and for the neuron 7 in the range $[-0.1, 0.1]$ (step of 0.01) and keeping fixed to 0 the stimuli for the other cells. The number of classes emerged is 24 for the 441 trials.

DOI: 10.1002/cta

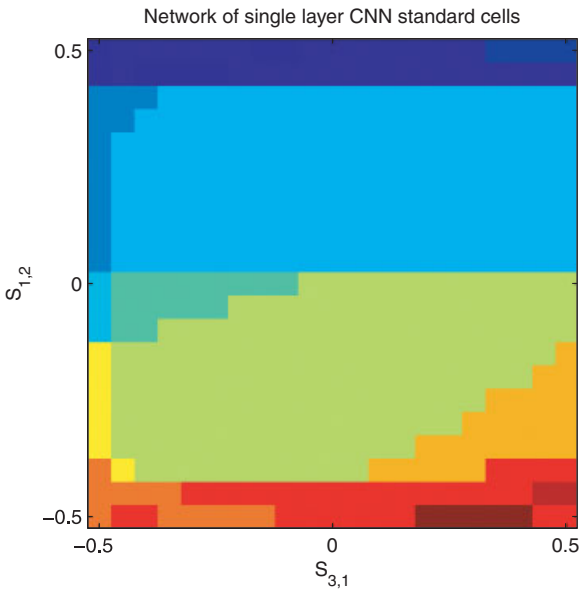

Figure 11. Network of single layer CNN standard cells: results of the simulation obtained varying the stimuli for the neuron 2 and for the neuron 7 in the range $[-0.5, 0.5]$ (step of 0.05) and keeping fixed to 0 the stimuli for the other cells. The number of classes emerged is 14 for the 441 trials.

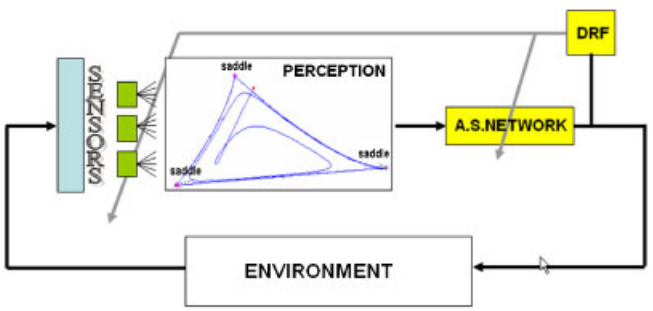

Figure 12. Functional block diagram of the implemented framework.

and the heavy regularity of the geometry of the classification regions (Figure 9) suggests to use the FHN system for perceptual purpose [21].

The perceptual architecture is the same introduced in [17] and is made up of four main blocks (Figure 12): the sensing block that receives the external stimuli; the perceptual block that builds up a representation of the environment; the action selection table that triggers an action to the effectors; the difference of reward function (DRF) block, which evaluates the goodness of actions driving the learning process.

In the following we will refer to *iteration* to indicate a single robot action, while we will call *cycle* the whole set of iterations between two consecutive target findings.

DOI: 10.1002/cta

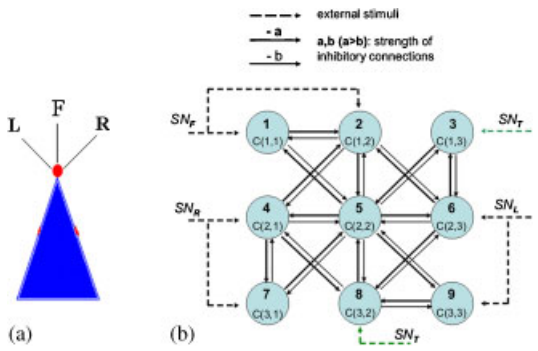

Figure 13. (a) Position of the distance sensors on the robot: F, L, R are front, left and right side sensors, respectively and (b) structure of the FHN network and input for the neurons. Six cells are injected with a current proportional to the obstacle stimuli (front, left and right side obstacle sensors), while two other cells have an input current related to the phase between target and robot orientation.

4.1. The control block

The simulated robot is provided with three distance sensors (covering the front, left and right side of the robot) for the detection of obstacles (Figure 13a). Another sensor provides the angle between the robot orientation and the robot–target direction. This information could come in different ways depending on the specific task: it could come from a network that processes the auditory stimuli in cricket phonotaxis [22], or it could be extracted from the visual field by using landmarks.

Each sensing stimulus is the input for a sensing neuron (SN) endowed with a piece-wise linear activation function made up of 10 amplitude-varying steps. The amplitudes of the steps are learned in an unsupervised way, as explained in the following. Finally, each output of the SNs is the input for a cell of the WLC network representing the perceptual core.

The aim of the perceptual core is to build up, on the basis of the incoming stimuli, abstract representations of the external world that trigger specific actions. These mechanisms are modulated by the experience thanks to learning. The perceptual core is a 3×3 cellular nonlinear system with FHN neurons and the connection matrix able to generate a WLC behavior presented in the previous section. The coded sequence obtained at each step represents the class of the current set of stimuli.

The choice of the cells, where to inject the current input $S_{i,j}$ (Figure 13(b)), is discussed in [21]. To finely represent different environmental situations, it would be feasible to have a large number of spatiotemporal patterns (i.e. sequences), but the pattern control would risk to be less effective. As seen in the previous section, using fixed connections between the cells represent a trade-off between the amount of different sequences and easiness of control, because this limits the number of possible classes from $e \cdot (8!)$ to around two hundreds, bounding the output of the SNs in the range $[0, 0.1]$.

We let the WLC network evolves and, once a sequence is recognized, its code is stored in a *sequence vector* at the first occurrence.

The use of a WLC network allows us to fuse lots of heterogeneous sensory information into a spatiotemporal pattern. At each step, the information coming from sensors is fused to form a unique abstract representation of the environment.

DOI: 10.1002/cta

The action selection network associates each element q of the pattern vector with an action A_q. An action consists of two elements, the module and the phase of the robot movement setting, respectively, the translational step and the rotation. Each element q of the pattern vector is connected to two weights, $w_{q,m}$ and $w_{q,p}$, representing, respectively, module and phase of the action A_q. In this paper, we keep the fixed weight $w_{q,m} = w_m$ for all the patterns and vary only the $w_{q,p}$ through a reward-based reinforcement learning implemented by a simplified motor map (MM) [23, 24]. Emulating the associative learning in animals, we determine the goodness of an action by means of a reward function (RF) defined as follows:

$$\mathrm{RF} = -\sum_i k_i \cdot f_i(D_i) - h \cdot f_{\mathrm{T}}(|\phi_{\mathrm{T}}|) \tag{15}$$

where D_i is the distance between the robot and the obstacle detected by the sensor i $(i = F, R, L)$, Φ_{T} is the angle between the robot orientation and the direction connecting robot and target, while k_i and h are positive constants determined during the design phase. The aim of the learning algorithm is to maximize the RF: small absolute values in Equation (15) indicate good situations for the robot. The goodness of an action performed at the step t is provided by $\mathrm{DRF}(t) = \mathrm{RF}(t) - \mathrm{RF}(t-1)$. A positive (negative) value for DRF indicates a successful (unsuccessful) action. Successful actions are followed by reinforcement, like in Skinner's experiments [25].

SNs are responsible for transforming the incoming stimuli into inputs for the WLC network, which will show a spatiotemporal sequence of activation represented by the timing of the bursting activity of the neurons.

Our choice for the SNs activation function consists in an increasing function constituted of 10 amplitude-varying steps, θ_i $(1 \leqslant i \leqslant 10)$, covering the whole input range $[-1, 1]$. At the beginning of the learning phase, all the steps have zero amplitude. At each step, if the performed action has positive effects (DRF$>$0), then the amplitude of the step does not change. Otherwise, when the action proves to be negative, the amplitudes of the steps are modified randomly in order to modulate the association between stimuli and resulting spatiotemporal patterns. The idea is that, when the action associated with the previous situation is no longer able to make the robot succeed in accomplishing the current task, a new pattern/situation should emerge and the suitable action to this new environmental condition has to be learned by the robot. In such a way the sensorial stimuli will be divided into classes associating different situations with patterns that generate positive actions. The output of the SNs is in any case bounded in the range $[0, 0.1]$. More details on the whole mathematical model are given in [17] and in [21].

4.2. Simulation results

The software simulation environment allows to create an arena constituted by walls, obstacles and targets. Moreover, in the arena a robot, equipped with a distributed sensory system, can be simulated.

The dimensions of the arena are 380×313 pixels and it is filled by obstacles and a target. The simulated robot is equipped with three distance sensors placed in the left, front and right side of the robot and one target sensor. The left and right side sensors are at 45° from the longitudinal axis of the robot (Figure 13(a)). All the distal sensors can detect obstacles within a limited range of 50 pixels and a visual field of $[-10°, 10°]$. The simulated target is a sound source that can be sensed by two microphones providing information on the angle between the robot orientation and the robot–target direction.

DOI: 10.1002/cta

All the sensor outputs are scaled in the range $[-1, 1]$. In this application, we design a linear RF; hence, it components (15) are defined as:

- $f_F(D_F) = -(1-0.5(D_F+1))$
- $f_L(D_L) = -(1-0.5(D_L+1))$
- $f_R(D_R) = -(1-0.5(D_R+1))$
- $f_T(\Phi_T) = -1*|\Phi_T|$

where D_F, D_R, D_L are the scaled distances detected by the sensors. In the following simulations, the choice for the other parameters in Equation (15) was: $k_F = 70$, $k_L = k_R = 40$ and $h = 40$. In this way, more importance is given to the contribution of the obstacle information than the target one because it is crucial for avoiding collisions. In particular, the output coming from the front side obstacle sensor has the greatest weight in the RF. Through the definition of this RF, we give to the robot knowledge about the task to be fulfilled, but it has no *a priori* knowledge about the correct way to interact with the environment. Thus, the phase of the actions associated with each pattern is randomly initialized within the range $[-0.05\,\text{rad}, 0.05\,\text{rad}]$. As far as the simulated robot is concerned, the task given to the robot consists in aiming a sound source avoiding obstacles.

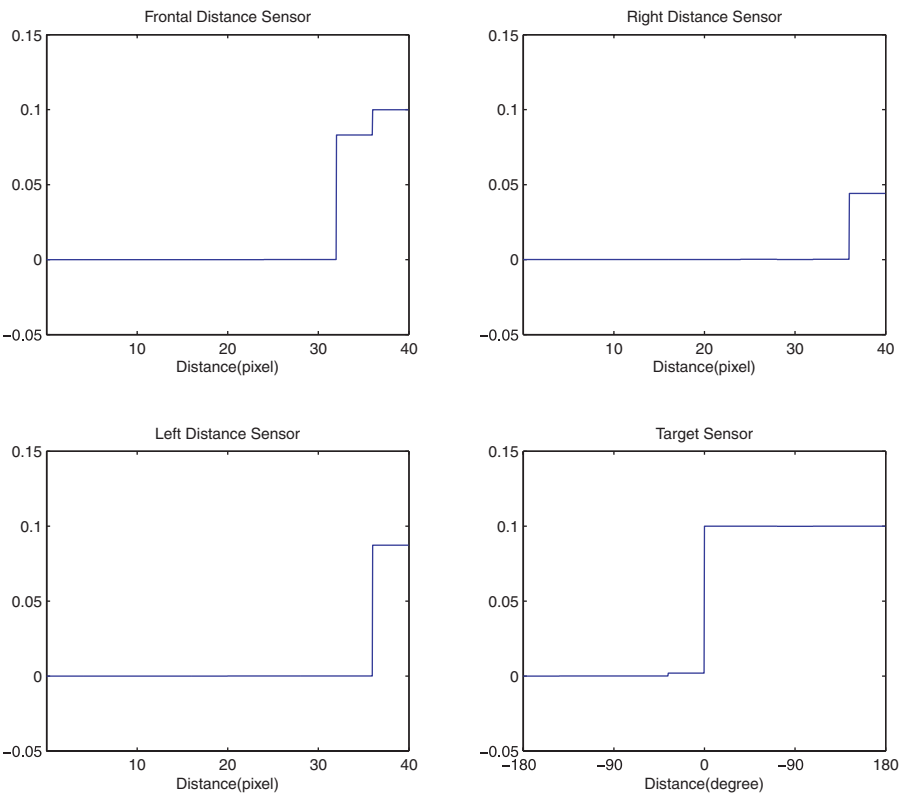

Figure 14. Result of the unsupervised learning of the amplitudes of the steps of the *SNs* activation functions related to the left, right and frontal distance sensor, and to the target sensor associated with the phase of the sound source.

DOI: 10.1002/cta

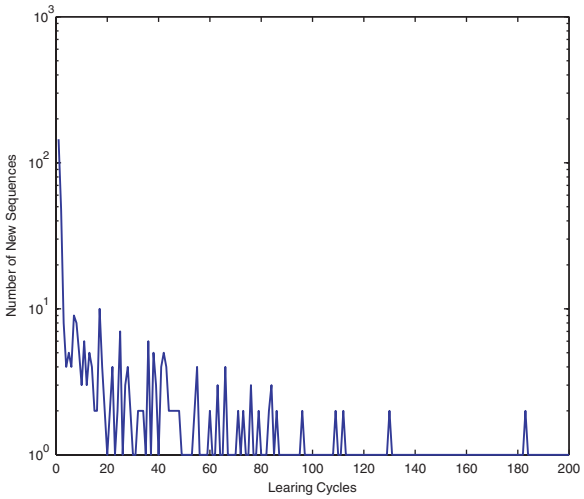

Figure 15. Number of new sequences emerged during the learning phase.

The learning phase consists of 200 trials, where a trial is made of a limited sequence of actions allowing to reach the target.

At the beginning of the learning phase, the robot performs random actions due to the random initialization of the phase weights $w_{q,p}$, which determine the robot heading. During the learning process, the MM-like algorithm corrects the action associated with each pattern. After the learning phase, the simulated robot has acquired the ability to aim the sound source. Figure 14 shows the result of learning the amplitudes of the steps for all the SNs activation functions, whereas Figure 15 figures out how the number of new sequences in time decreases with the learning evolution demonstrating the convergence of the learning at the afferent layer. In terms of robot performance, the result of the learning consists in a strong reduction of the number of the robot's steps between two consecutive target findings as shown in Figure 16. Once having completed the learning phase, the testing phase shows the ability acquired to safely navigate and reach the audio (target) source in presence of obstacles. In the testing phase, the agent has been able to find the audio source starting from different initial conditions without hitting obstacles. Figure 17 reports some examples of such a behavior.

Further investigations will be devoted to understand how the emerging sequences could be associated, through learning, with motor sequence able to achieve more complex tasks.

5. CONCLUSIONS

In this paper, we review the analytical principle of the WLC network in the case of Lotka–Volterra system to serve as the computational core within a more complex spatial–temporal architecture for action-oriented perception. Moreover, we have extended the WLC behaviour to the class of the CNN after having formalized a *WLC-like* behavior based on heuristic considerations, due to the lack in theoretical results. In order to assess the suitability of the approach, we took into account in this paper a number of different cells, investigating their capability to work as realtime

DOI: 10.1002/cta

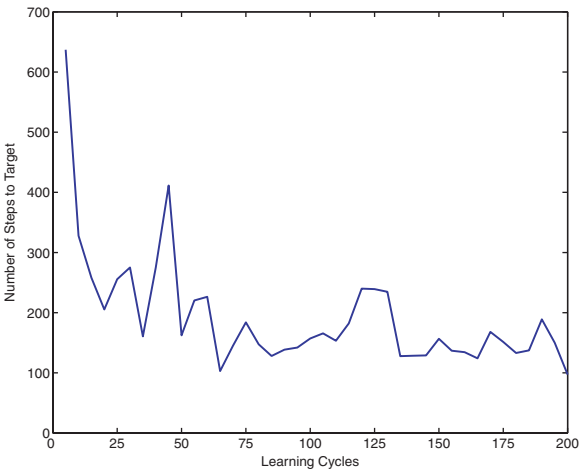

Figure 16. Number of steps between two consecutive target findings: each of the 20 values represents the mean number of steps needed to find a target in a window of five consecutive target findings.

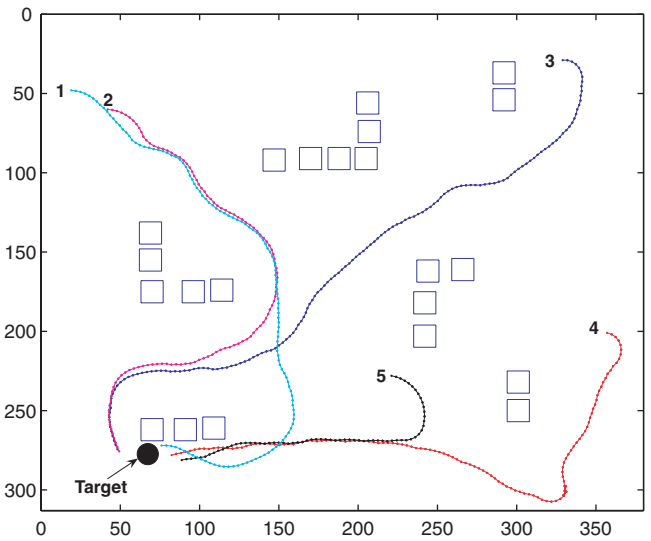

Figure 17. Trajectory followed in the test after learning. The agent reaches the audio source starting from five different initial conditions.

input signal classifiers. We have shown how a suitable choice for the connection parameters in a $2D$ 3×3 CNN can lead to a WLC-like behavior for various kinds of cells. Subsequently, we analyzed the characteristics of WLC–CNN networks built using FHN neurons, single layer CNN standard cells and IZH neurons, outlining their performances in terms of robustness and number of classes. This feature is, in the case of WLC networks, much greater than a multistable

DOI: 10.1002/cta

network due to the temporal coding, more powerful than coding with attractors. In all the presented cases, the dynamics obtained exhibits repetitive time-locked activity of the cells, in analogy to the polichronization of a spiking network proposed by IZH [26]. We found that only the FHN neurons present features of both high capability and good robustness, while the single layer CNN standard cells are very robust, but poor in terms of number of classes. The natural application is to the classification problem, but we have also shown the application to a recently designed perceptual architecture, where the WLC net represents the core for the classification of external stimuli. The huge, in principle, number of different spatiotemporal sequences, depending only on input signals, guarantees robustness to the emerging attractor, which becomes, once associated to an action, 'the mirror' of the environment for motor purposes. This new application of the WLC-based perceptual motion, uses these networks as sequence generators, that reflect the spatial–temporal motion of a roving robot within a physical world. Thus, the robot navigation task can be seen as the spatial–temporal sequence of WLC generated codes, constituting the robot internal representation of the external world.

ACKNOWLEDGEMENTS

The authors acknowledge the support of the European Commission under the EU projects SPARK I and II and the MIUR-PRIN project: 'Nonlinear dynamic network: analysis and application', 2006–2008.

REFERENCES

1. Meredith M. Patterned response to odor in mammalian olfactory bulb: the influence of intensity. *Journal of Neurophysiology* 1986; **56**:572–597.
2. Christensen T, Hildebrand J. Male-specific, sex pheromone-selective projection neurons in the antennal lobes of the moth *Manduca sexta*. *Journal of Comparative Physiology A* 1987; **160**:553–569.
3. Laurent G, Wehr M, Davidowitz H. Temporal representations of odors in an olfactory network. *The Journal of Neuroscience* 1996; **16**(12):3837–3847.
4. Mazor O, Laurent G. Transient dynamics versus fixed points in odor representations by locust antennal lobe projection neurons. *Neuron* 2005; **48**:661–673. DOI: 10.1016/j.neuron.2005.09.032.
5. Wessnitzer J, Webb B. Multimodal sensory integration in insects—towards insect brain control architectures. *Bioinspiration and Biomimetics* 2006; **1**:63–75.
6. Rabinovich M, Volkovskii A, Lecanda P, Huerta R, Abarbanel HDI, Laurent G. Dynamical encoding by networks of competing neuron groups: winnerless competition. *Physical Review Letters* 2001; **87**(6):068102-1.
7. Afraimovich VS, Rabinovich MI, Varona P. Heteroclinic contours in neural ensembles and the winnerless competition principle. *International Journal of Bifurcation and Chaos* 2004; **14**(4):1195–1208.
8. FitzHugh R. Impulses and physiological states in theoretical models of nerve membrane. *Biophysics* 1961; **7**:1.
9. Izhikevich EM. Simple model of spiking neurons. *IEEE Transactions on Neural Networks* 2003; **14**:1569–1572.
10. Chua L, Yang L. Cellular neural networks: theory. *IEEE Transactions on Circuits and Systems* 1988; **35**: 1257–1272.
11. La Rosa M, Caruso E, Fortuna L, Frasca M, Occhipinti L, Rivolia E. Neuronal dynamics on FPGA: Izhikevich's model. *Proceedings of SPIE*, Sevilla, Spain, 2005.
12. Carmona R, Jiménez-Garrido F, Domínguez-Castro R, Espejo S, Rodríguez-Vázquez A. Bio-inspired analog VLSI design realizes programmable complex spatio-temporal dynamics on a single chip. *Proceedings of Design, Automation, and Test in Europe Conference*, IEEE Computer Society, Washington, DC, U.S.A., 2002; 362–366.
13. Xavier-de-Souza S, Suykens JAK, Vandewalle J. Learning of spatiotemporal behaviour in cellular neural networks. *International Journal of Circuit Theory and Applications* 2006; **34**(1):127–140.
14. Tetzlaff R, Niederhöfer C, Fischer P. Automated detection of a preseizure state: non-linear EEG analysis in epilepsy by cellular nonlinear networks and volterra systems. *International Journal of Circuit Theory and Applications* 2006; **34**(1):89–108.

15. Petrás I, Gilli M. Complex dynamics in one-dimensional CNNs. *International Journal of Circuit Theory and Applications* 2006; **34**(1):3–20.
16. Földesy P, Zarándy Á, Rekeczky C, Roska T. Digital implementation of cellular sensor-computers. *International Journal of Circuit Theory and Applications* 2006; **34**(4):409–428.
17. Arena P, Crucitti P, Fortuna L, Frasca M, Lombardo D, Patané L. Turing patterns in RD-CNNs for the emergence of perceptual states in roving robots. *International Journal of Bifurcation and Chaos* 2007; **10**(1):107–127.
18. Van Den Driessche P, Zeeman M. Three-dimensional competitive Lotka–Volterra systems with no periodic orbits. *SIAM Journal of Applied Mathematics* 1998; **58**:227–234.
19. Chauvet E, Paullet JE, Previte JP, Walls Z. A Lotka–Volterra three-species food chain. *Mathematics Magazine* 2002; **75**(4):243–255.
20. Arena P, Bedia MG, Fortuna L, Lombardo D, Patanè L, Velarde MG. Spatio-temporal patterns in CNNs for classification: the winnerless competition principle. *Proceedings of CNNA2006*, Istanbul, Turkey, 2006.
21. Arena P, Fortuna L, Lombardo D, Patanè L, Velarde MG. The WLC principle for action-oriented perception. *Proceedings of SPIE*, *Europe*, 2007.
22. Webb B, Scutt T. A simple latency dependent spiking neuron model of cricket phonotaxis. *Biological Cybernetics* 2000; **82**(3):247–269.
23. Schulten K. Theoretical biophysics of living systems. In *Neural Computation and Self-organizing Maps*: *An Introduction*, Ritter H, Martinez T, Schulten K (eds). Addison-Wesley: New York, 1992.
24. Arena P, Fortuna L, Frasca M, Sicurella G. An adaptive, self-organizing dynamical system for hierarchical control of bio-inspired locomotion. *IEEE Transactions on Systems*, *Man and Cybernetics*, *Part B* 2004; **34**(4):1823–1837.
25. Skinner BF. *About Behaviorism*. Alfred Knopf: New York, 1974.
26. Izhikevich EM. Polychronization: computation with spikes. *Neural Computation* 2006; **18**:245–282.

DOI: 10.1002/cta